International Journal of Thermofluid Science and Technology (2023)
Volume 10, Issue 2, Paper No. 100201
https://doi.org/10.36963/IJTST.2023100201
Research Article

Influences of electrical conductivity of the cylindrical walls on heat transfer enhancement of nanofluid swirling flow

Fateh Madani[1], Brahim Mahfoud[*,2], Hibet Errahmane Mahfoud[3]

[1]*Department of Mechanical Engineering, University of Blida 1, 09000, Algeria*
[2]*Department of Mechanical Engineering, University of UAMO-Bouira, 10000, Algeria*
[3]*Technicum of Collo, National Education –Skikda, 21000, Algeria.*

ARTICLE INFO

Received: 23 Mar. 2023;
Received in revised form:
03 Apr. 2023;
Accepted: 10 Apr. 2023;
Published online:
15 Apr. 2023

Keywords:
Electric conductivity
Enhancement heat transfer
Nanofluid
swirling flow
Magnetic field

ABSTRACT

The swirling nanofluid flow driven by a revolving bottom disk of a cylindrical container under magnetic field effect and temperature gradient is examined in this study. The effects of the electrical conductivity of cylindrical walls' on heat transfer enhancement are quantitatively investigated. The finite volume approach is used to solve the governing equations under the appropriate assumptions. This study considers four cases of combined electric conducting and insulating walls. The solid nanoparticle (copper) with volume fraction (ϕ = 0.1) is added to water. Calculations were done for fixed Reynolds number (Re=1000), Richardson number ($0 \leq Ri \leq 2$), and various Hartmann numbers. The mean Nusselt number decreased as the Richardson number increased owing to stratification layers. These latter restrict heat exchanges between the cylinder's hot and cold zones. The results show that within a particular range of Hartmann numbers, the Nusselt number increases, especially when the revolving lid is electrically conducting. The best heat transfer occurs when all of the walls are electrically conductive, which results in a 100% improvement at low Richardson values. Finally, the electrical conductivity of the revolving lid was a key factor in enhancing heat transfer.

1. Introduction

Several scientific studies suggest that nanofluids are a new form of heat transfer fluid that is better suited for cooling technologies [1-4]. Thermal evaluation of a solar concentrating system using CNT nanoparticles and a complicated helical turbulator has recently been studied by [5]. Recently [6] studied solar systems equipped with an innovative turbulator and a hybrid nanofluid. Studies have recently been focusing on energy storage and reduction of energy consumption incorporated with nanofluid [7-11].

In addition, other studies in MHD demonstrate that applying a magnetic field to electrically conductive fluids provides some stability to turbulent flows [12-17]. Recently studies [18-20] have investigated thermal management and performance enhancement using the combined impacts of magnetic field and phase change material for hybrid convection nano-liquids through a 3D vented cylindrical cavity.

[*]Corresponding e-mail: *b.mahfoud@univ-bouira.dz* (Brahim Mahfoud)

Nomenclature

B	magnitude of the external magnetic field, Tesla	Greek symbols	
E	electric charges	α	thermal diffusivity of the fluid, m^2/s
F_L	Lorentz force	β	thermal expansion coefficient, 1/K
H	height of the cylinder, m	ν	kinematic viscosity of the fluid, m^2/s
Ha	Hartmann number	λ	thermal conductivity (w/ m. C)
J	dimensionless current density	ρ	density of the fluid (kg/m^3)
Nu	Nusselt number	σ	electric conductivity (Ω /m)
$\overline{Nu}$	average Nusselt number	Φ	dimensionless electric potential
P	dimensionless pressure	Ω	angular velocity, rad/s
Pr	Prandtl number	Ψ	non-dimensional stream function
R	radius, m	Θ	dimensionless temperature
Re	Reynolds number	τ	dimensionless time
Ri	Richardson number	ϕ	volume fraction
$\boldsymbol{V}$	velocity vector	*Subscripts symbols*	
T	Temperature	c_r	critical value
$u, v,$	dimensionless axial, radial velocities	f	fluid
w	dimensionless azimuthal velocity	p	solid phase

New models and techniques for hybrid nanofluids can be quite advantageous in a variety of sectors where cooling technologies are critical [21]. Experimental relationships of effective thermophysical characteristics may be trusted and adaptable in theoretical and mathematical modeling of hybrid nanofluid flows[22]. The steady laminar MHD flow of a magnesium oxide-silver/water hybrid nanofluid along a horizontal slim needle with thermal radiation have carried out by Dinarvand et al. [23] by considering dual solutions. Dinarvand et al. [24] confirm that the porosity and the magnetic effect amplify heat transfer rate, while the unsteadiness parameter has a reducing effect on heat transfer rate in troubled conditions. The effect of spinning parameters and nanoparticles masses on the hydrodynamics and thermal boundary layers behavior are presented in [25].

Another study considers a ferro-hybrid nanofluid on a non-linear stretch permeable sheet in a porous medium [26]. A hybrid nanofluid with radiation and MHD effects has been semi-analytically studied in [27]. The viscoelastic nanofluid past a circular cylinder with sinusoidal radius variation has been discussed in [28]. Finally, the stagnation point of the three-dimensional MHD considering a hybrid aluminium-copper/water nanofluid was described by Jabbaripour et al.[29]

Mahfoud [30,31] investigated the effects of the electrical conductivity of cylindrical walls on both heat transfer enhancement in nanofluid swirling flow and fluid layers produced in a cylindrical container.

For small and intermediate cylinders, electromagnetic stabilization is recommended by putting a magnetic field on the swirling flow in the preferred direction [32,33]. The passage of electrically conductive fluid through the magnetic field causes the induced electric current (interaction of the convective roll with the magnetic). The forces emerge as a result of the magnetic field altering the flow of the fluid. In the area of the rotating lid, an equilibrium between centrifugal and viscous forces arises in the Ekman boundary layer.

Under the influence of a magnetic field, the latter is replaced by the Hartmann layer[34,35]. It is worth noting that when the spinning lid is electrically conductive, the fluid rotates through the inertial force of the bottom revolving disk [36]. Previous studies [37-39] support the use of a magnetic field to move from oscillatory instability to stable bifurcation. Devi and Devi [40] investigated the influence of Newtonian heating and Lorentz force on the flow of a three-dimensional hybrid Cu-Al2O3/water nanofluid across a stretched sheet. It was shown various characteristics of the same hybrid nanofluid flow from a cavity [41]. The study of nanofluid behavior in rotating media under magnetic field effect has lately been an appealing focus for researchers, combining numerical and analytical approaches with nanofluid and magnetic fields. It is worth noting that the reviewer [42, 43] has adequately summarized the latest works that link nanofluid with a magnetic field. They demonstrated that although solid particle concentration and buoyancy increase the temperature gradient, increasing the magnetic field lowers it.

Previous publications associating nanofluid and magnetic field are interested in the behavior of solid particle concentration and buoyancy force under the effect of magnetic field when all solid walls are electrically insulating. But in the present work, the objective is to clarify the role of the wall's electrical conductivity on the flow dynamics and enhancement heat transfer.

The second objective is to identify the magnetic field intensity corresponding best to the enhancement heat transfer.

The third objective is to identify the best case among the four cases studied here that corresponds best to enhancement heat transfer.

A series of 2D numerical simulations are provided in this work to gain a better understanding of the impact that axial magnetic field and vertical temperature gradient have on swirling flow. The calculations were performed for two alternative scenarios: (1) all walls are electrically insulating, which was designed by (Walls-EI); (2) all walls are electrically conducting, which was designed by (Walls-EC) and two other combined cases designed by (Bottom-EC), and(Top-EC). The flow pattern and heat transfer are explained using the problem-defining parameters such as (*Ha*) Hartmann number, (*Ri*) Richardson number, and (*Re*) Reynolds number.

2. Flow Description and Model

The physical model is a cylindrical enclosure schematically displayed in Fig.1. The aspect ratio is H/R=2where R is the radius, and H is the height, respectively. The cylindrical enclosure is filled with nanofluid (Cu-Eau). The thermal equilibrium of the solid spherical copper particles (Cu) with the base fluid (water) is perfect. Results of numerical simulations are used in the model of Tiwari-Das nanofluid [44]. The nanofluid swirling flow is studied for a choice of nanoparticles (Cu) with solid volume fraction (ϕ=0.1). The upper stationary disk is kept at a high-temperature T_h, while the lower moving disk is kept at a low-temperature T_c($T_c < T_h$). The temperature difference between T_h and T_c causes the vertical temperature gradient. With constant angular velocity Ω, the bottom lid rotates. In addition, an axial magnetic field B is acting on the nanofluid container. The nanofluid's thermophysical properties are all constant (Table 1).

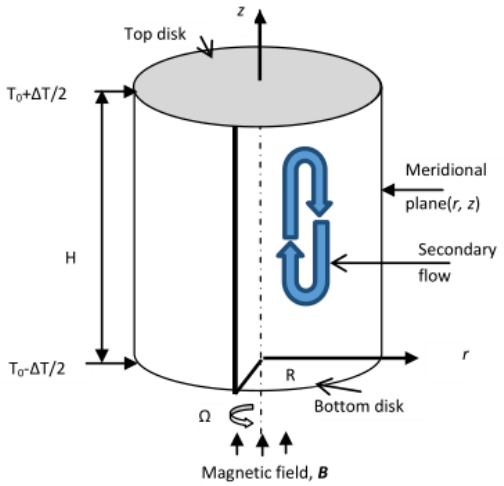

Fig. 1. The computational domain

The dimensionless governing equations are implemented via the following variant: Time ($1/\tau$), R for the length, (ΩR) for

velocities, the pressure is obtained by $\rho_{nf}(\Omega R)^2$, temperature, $\Theta = (T - T_0)/\Delta T$ and electric potential, $B_0 \Omega R^2$.

Continuity equation:

$$\frac{\partial (ru)}{\partial r} = -\frac{r \partial v}{\partial z} \tag{1}$$

Momentum equations (for r and z):

$$\frac{\partial u}{\partial \tau} + u\frac{\partial u}{\partial r} + v\frac{\partial u}{\partial z} - \frac{w^2}{r} = -\frac{\partial P}{\partial r} + \frac{1}{\mathrm{Re}_f}\left(\frac{\mu_{nf}\rho_f}{\mu_f \rho_{nf}}\right)\times \left(\frac{1}{r}\frac{\partial}{\partial r}\left(r\frac{\partial u}{\partial r}\right) + \frac{\partial^2 u}{\partial z^2} - \frac{u}{r^2}\right) + N_f\left(\frac{\sigma_{nf}\rho_f}{\sigma_f \rho_{nf}}\right)F_{Lr} \tag{2}$$

$$\frac{\partial v}{\partial \tau} + u\frac{\partial v}{\partial r} + v\frac{\partial v}{\partial z} = -\frac{\partial P}{\partial z} + \frac{1}{\mathrm{Re}_f}\left(\frac{\mu_{nf}\rho_f}{\mu_f \rho_{nf}}\right)\times \left(\frac{1}{r}\frac{\partial}{\partial r}\left(r\frac{\partial v}{\partial r}\right) + \frac{\partial^2 v}{\partial z^2}\right) + Ri_f\left(\frac{(\rho\beta)_{nf}}{\beta_f \rho_{nf}}\right)\cdot\Theta + N_f\left(\frac{\sigma_{nf}\rho_f}{\sigma_f \rho_{nf}}\right)F_{Lz} \tag{3}$$

Swirl equation:

$$\frac{\partial w}{\partial \tau} + u\frac{\partial w}{\partial r} + v\frac{\partial w}{\partial z} + \frac{uw}{r} = \frac{1}{\mathrm{Re}_f}\left(\frac{\mu_{nf}\rho_f}{\mu_f \rho_{nf}}\right)\times \left(\frac{1}{r}\frac{\partial}{\partial r}\left(r\frac{\partial w}{\partial r}\right) + \frac{\partial^2 w}{\partial z^2} - \frac{w}{r^2}\right) + N_f\left(\frac{\sigma_{nf}\rho_f}{\sigma_f \rho_{nf}}\right)F_{L\theta} \tag{4}$$

Energy equation:

$$\frac{\partial \Theta}{\partial \tau} + u\frac{\partial \Theta}{\partial r} + v\frac{\partial \Theta}{\partial z} = \frac{1}{\mathrm{Re}_f \cdot \mathrm{Pr}_f}\left(\frac{\alpha_{nf}}{\alpha_f}\right)\times \left(\frac{1}{r}\frac{\partial}{\partial r}\left(r\frac{\partial \Theta}{\partial r}\right) + \left(\frac{\partial^2 \Theta}{\partial z^2}\right)\right) \tag{5}$$

The electric potential equation:

$$\frac{1}{r}\frac{\partial}{\partial r}\left(r\frac{\partial \Phi}{\partial r}\right) + \frac{\partial^2 \Phi}{\partial z^2} = \frac{w}{r} + \frac{\partial w}{\partial r} \tag{6}$$

The Lorentz force is only a function of r and θ. They may be found by: $\boldsymbol{F_L = JXB}$, the dimensionless Lorentz forces in the r, z, and θ directions are respectively:

$$\begin{cases} radial\ force: F_{Lr} = -u \\ \text{axial force: } F_{Lz} = 0 \\ \text{azimuthale force: } F_{L\theta} = \frac{\partial \Phi}{\partial r} - \mathrm{w} \end{cases} \tag{7}$$

The dimensionless parameters characterizing this swirling nanofluid flow are:

$$\begin{cases} \text{Richardson number} Ri_f = \frac{\beta_f g \Delta T}{\Omega^2 R} \\ \text{Interaction parameter} N_f = \frac{Ha_f^2}{Re_f} \\ \text{Reynolds number: } Re_f = \frac{\Omega R^2}{\nu_f} \\ \text{Hartmann number: } \mathrm{Ha}_f = BR\sqrt{\sigma_f/\rho_f \nu_f} \end{cases} \tag{8}$$

The non-dimensional stream function ψ presents the velocity field (u, v), which is specified as:

$$r.u = \left(\frac{\partial \Psi}{\partial z}\right); \quad r.v = -(\partial \Psi/\partial r) \tag{9}$$

The local and average Nusselt numbers define as:

$$\begin{cases} Nu(r,\theta) = \frac{k_{nf}}{k_f}\left(\frac{\partial \Theta}{\partial z}\right)\Big|_{z=0\ or\ H} \\ \text{and} \\ \overline{Nu} = \left(\frac{1}{\pi}\right)\int_0^1 \int_0^{2\pi} Nu\,(r,\theta) r d\theta dr\,, \end{cases} \tag{10}$$

Table 1. Properties of nanofluids from Sheikholeslami et al. [3], with ϕ (volume fraction), f (fluid) and p (solid phases)

Thermo-physical property	Relation
Density	$\rho_{nf} = (1-\phi)\rho_f + \phi\rho_P$
Dynamic viscosity	$\mu_{nf} = \frac{\mu_f}{(1-\phi)^{2.5}}$
Heat capacity	$(\rho C_p)_{nf} = (1-\phi)(\rho C_p)_f + \phi(\rho C_p)_P$
Expansion coefficient	$(\rho\beta)_{nf} = (1-\phi)(\rho\beta)_f + \phi(\rho\beta)_P$
Diffusivity	$\alpha_{nf} = k_{nf}/(\rho C_p)_{nf}$
Conductivity	$k_{nf} = k_f\left[\frac{(k_f + 2k_f) - 2\phi(k_f - k_p)}{(k_p + 2k_f) + \phi(k_f - k_p)}\right]$
Electrical conductivity	$\sigma_{nf} = \sigma_f\left[1 + \frac{3(\frac{\sigma_p}{\sigma_f} - 1)\phi}{(\frac{\sigma_p}{\sigma_f} + 2) + \phi(\frac{\sigma_p}{\sigma_f} - 1)}\right]$

The axisymmetric boundary condition is shown in Table.2. The nanofluid is at rest at τ = 0. Note that the boundary conditions corresponding to electric potential are summarized in Table 3

Table 2 The boundary conditions

Boundary	u	v	w	Θ
r=0, 0≤ z ≤ 2	$u = 0.$	$\frac{\partial v}{\partial r} = 0.$	$w = 0.$	$\frac{\partial \Theta}{\partial r} = 0$
r=1, 0≤ z ≤ 2	$u = 0.$	$v = 0.$	$w = 0.$	$\frac{\partial \Theta}{\partial r} = 0$
z=0, 0≤ r ≤ 1	$u = 0.$	$v = 0.$	$w = r$	$\Theta = -\frac{1}{2}$
z=2, 0≤ r ≤ 1	$u = 0.$	$v = 0.$	$w = 0.$	$\Theta = \frac{1}{2}$

Table 3. The boundary conditions used for the electrical potential

Boundary	EI-Walls	EC-Walls	EC-Bottom	EC-Top
r=0, 0≤ z ≤ 2	$\frac{\partial \Phi}{\partial r} = 0.$	$\frac{\partial \Phi}{\partial r} = 0$	$\frac{\partial \Phi}{\partial r} = 0$	$\frac{\partial \Phi}{\partial r} = 0.$
r=1, 0≤ z ≤ 2	$\frac{\partial \Phi}{\partial r} = 0.$	$\Phi = \frac{1}{2}$	$\frac{\partial \Phi}{\partial r} = 0$	$\frac{\partial \Phi}{\partial r} = 0.$
z=0, 0≤ r ≤ 1	$\frac{\partial \Phi}{\partial z} = 0.$	$\Phi = \frac{r^2}{2}$	$\Phi = \frac{r^2}{2}$	$\frac{\partial \Phi}{\partial z} = 0.$
z=2, 0≤ r ≤ 1	$\frac{\partial \Phi}{\partial z} = 0.$	$\Phi = \frac{1}{2}$	$\frac{\partial \Phi}{\partial z} = 0.$	$\Phi = 0.$

3. Numerical Method

The mathematical equations (1-6) were solved using the finite difference method [45]. To discretize the convection and diffusion terms, a global second-order technique is applied. SIMPLER algorithm [46] was used to eliminate the coupling between pressure and velocity. The resultant system of algebraic equations is then solved using the Thomas Algorithm for Tridiagonal Matrix (TDMA). The following is the solution:

- Eqs. (1), (2), and (3) are first solved to provide pressure, radial velocity, and axial velocity.
-The swirl velocity is then calculated using Eq. (4).
- The temperature Θ and the potential Φ are subsequently computed from Eqs. (5) and (6), respectively.
-Steps 1–2 are repeated until convergence is achieved.

The various scalar and vector quantities associated with the ensemble of equations are discretized on a non-regular grid and solved on the (r; θ; z). The characteristics of the MHD swirling flow and boundary layers must be examined for a successfully solved numerical simulation. For instance, increasing Ha leads to smaller Hartmann layers of thickness ~1/*Ha* at the walls normal to the magnetic field. As a result, non-uniform grids based on geometric progressions of ratio 1.05, should be employed. In this context, we used a grid of 100×200 nodes to assure numerical stability.

4. Results and Discussion

Four cases were studied in this paper to identify the best case among and the maximum magnetic field intensity corresponding to the enhancement heat transfer, these cases are: all walls are electrically insulating (Walls-EI), all walls perfectly are electrically conducting (Walls-EC), only bottom disk is conducting (Bottom-EC), and the only top disk is conducting (Top-EC). The numerical simulation was carried out for a constant aspect ratio equal to 2, a fixed rotation rate Re=1000, a temperature difference range specified by (0≤Ri≤2), a Hartmann number in the range of 0 to 60, and a volume proportion of solid nanoparticles of copper (ϕ = 0.1).

4.1 Validation

The first comparison shown in Fig.2 (a) has been made with the numerical results of Aminossadati and Ghasemi [2] which present the profile of local Nusselt number along the heat source for various solid volume fractions (Cu–Water, Ra = 10^5 , D = 0.5 and B = 0.4).

The second comparison has been made with the numerical results due to Sheikholeslami et al. [3] as shown in Fig.2 (b). The comparison evaluates the effect of the magnetic parameter on the Nusselt number (Nu). The flow of nanofluids and heat transfer in a rotating system between two horizontal plates are investigated in this work. When the stretched sheet is the bottom plate and a solid permeable is the top plate, the comparison is conducted using the Reynolds number (Re = 1), injection parameter (λ= 1), rotation parameter (Kr = 1), and nanoparticle volume fraction parameter (ϕ=0.05 and 0.1). This comparison demonstrates a high agreement.

Third, magnetic effects on nanofluid flow were compared to the numerical study of Shafiee et al.[4]. In this comparison, numerical simulation studied the effects of a magnetic field produced in a porous media with a

volume fraction of 0.2 water/Al_2O_3 nanofluid inside the cylinder was investigated. The results of this comparison are presented in Fig. 3c for performance elevation criteria. According to the results, the maximum difference was smaller than 2%, which is considered negligible for a numerical study, indicating a good agreement between the results.

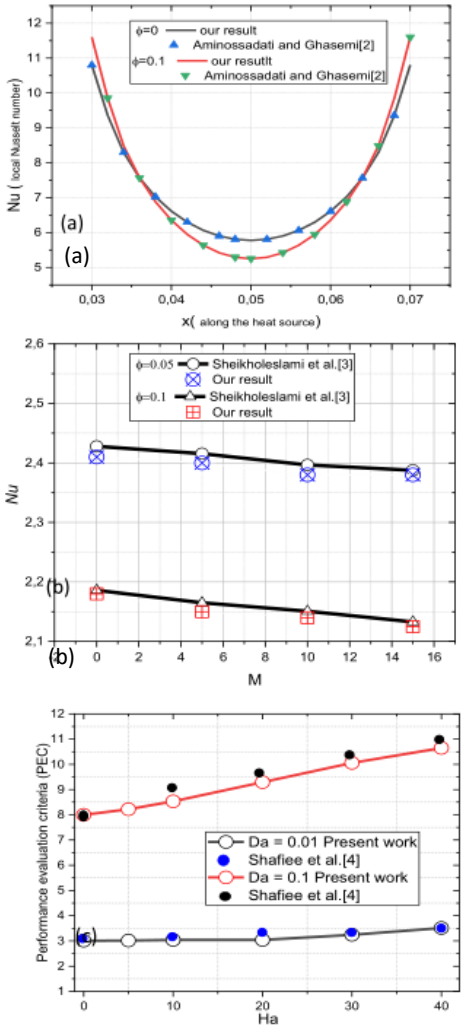

Fig. 2. Comparison with (a) the numerical result of Aminossadati and Ghasemi [2], (b) the numerical results of Sheikholeslami et al. [3]; the numerical results of Shafiee et al. [4].

4.2 Magnetic Effect on swirling flow behavior

First and foremost, it is to define the situation in which all of the enclosure's walls are electrically insulated. In this example, a series of simulations will be built that include increasing the Hartmann number, Ha = 10, 20, and 60. (Fig.3). The effect of increasing the amplitude of the magnetic field on the formation of nanofluid layers is depicted in Fig.3. The swirling flow of nanofluid in the presence of a magnetic field produces an induced current, which interacts with the magnetic field in turn. Then a Lorentz force in the opposite direction of the flow would be created. Lorentz force may efficiently restrict flow produced by temperature gradients and is suitable for multi-layer formation.

In the case of Ha=10, the hydrodynamic streamlines graphs reveal three layers, with the center layer having counter-flow recirculation. When Ha is raised to Ha=20, some intriguing alterations are detected in the intermediate layer. The streamlines clearly illustrate that the size of the middle counter-flow recirculation zone decreases while the size of the bottom cell increases. For Ha=60, the cell formed in the recirculation zone near the lower disc now comprises a major portion of the cylinder, but the countercurrent recirculation cell is considerably smaller and concentrated in the domain's center.

The flow pattern is seen in the second column when the top is electrically conductive (Top- EC). The flow pattern for Ha=10 and Ha=20 is somewhat similar to that of an insulating wall with three levels and countercurrent recirculation in the center. In the instance Ha=60, Ψ_{max} becomes 0.0025, the cell in the middle is larger than in the preceding example, and the latter compresses somewhat and is concentrated in the center of the container.

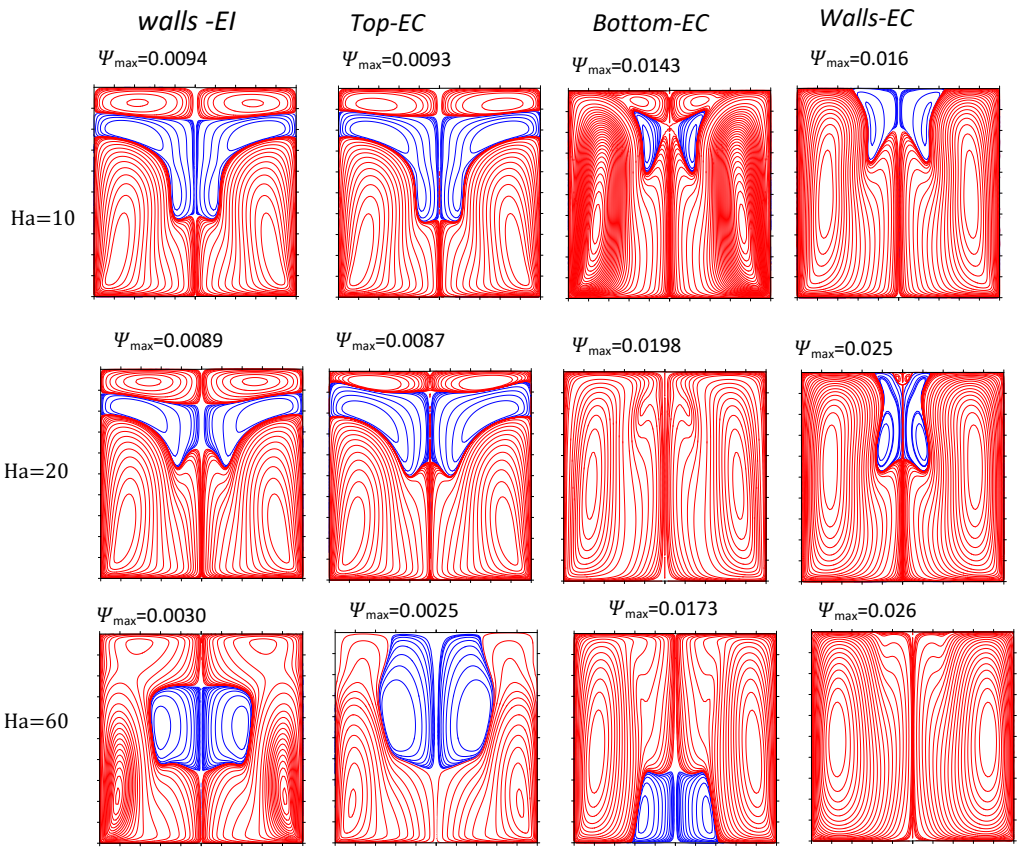

Fig. 3. Streamlines for progressively increasing Hartmann numbers when *Ri*=0.2 and different cases.

The flow pattern in the (Bottom-EC) case is observed in the third column of Fig.3. The electric conducting wall posits that the electric potential does not vary across the wall, implying that the wall current density is tangential to the wall. Note that the Hartmann layer disappears when the bottom wall is electrically conductive, and then, the fluid moves through the inertial force.

In the case of Ha=10, the hydrodynamic streamline charts reveal a separation bubble. The second cell is produced in the center-top at Ha=10. As a result, a modest magnetic field (Ha=20) is required to achieve a particular level of nanofluid flow stability. Furthermore, as Ha grows, the Ψ_{max}rises to a maximum which is 0.0183 at Ha = 30, and then falls till Ha = 60.

Column four of Fig.3 depicts the scenario when all of the container's walls are electrically conducting, in which one separation bubble emerges near the top disk at Ha = 10, decreases to Ha = 20, travels to the center at Ha = 30, and ultimately dissipates at Ha = 60. At Ha = 60, the maximum decrease occurs.

4.3 Heat Transfer without magnetic field

Figure 4 compares the local Nusselt number profile (dotted line for nanofluid) to (solid line for pure water) for different Richardson numbers at the upper disk (red color) and lower disk (black color). In Fig. 3a, the Nusselt number traced in the bottom disk achieves its maximum at r = 0, which is 12.8 for pure water and 18.67 for nanofluid when Ri=0.01. When moving in the direction of the side wall, a reduction is noted until r = 1.0. The Nusselt number on the top disk reaches its maximum value of 8.55 for pure water and 12.07 for nanofluid at r=0.72.

When Ri = 0.05, the heat transfer rate slows (see Fig. 4b), and when Ri = 0.1, the fluid layers thermally condense, isolating the upper area where conduction dominates heat transfer

(see Fig. 4c). In both circumstances, the local Nusselt number approaches a nearly constant value.

This tendency is most conspicuous at the top disk when Ri=0.5 (Fig.4d). For the bottom disk, the local Nusselt number is largest at r = 0 and decreases with the radius toward the sidewall. For all the values of Ri computed, the local Nusselt number has the largest values for nanofluid compared to pure water.

Without magnetic field, pure water and nanofluid are compared as the average Nusselt achieved by raising Richardson's number (Fig.5). The latter figure illustrates that Nusselt drops monotonically as Ri increases, approaching the conduction limit. It appears that (Nu) achieves an extreme value when Ri = 0 and is 7.99 for pure water, while it reaches an extreme value when Ri = 0 and is 10.66 for nanofluid flow. When Ri=0, the flow is dominated by a single layer, and the average Nusselt value reaches its maximum. The conflict between the two forces viscosity and buoyancy becomes increasingly crucial as Ri increases.

The heavier cold fluid accumulates near the cold disk at the bottom, while the warmer, lighter liquid floats above near the top disk. In this case, the accumulated liquid layers resist the rotation generated by the rotating lid, causing a decrease in the horizontal net transmission. The number of layers affects the heat transfer, as they act as thermal insulation.

It is clear from the preceding that adding nanoparticles to pure water increases the value of the Nusselt number. We find that adding nanoparticles to water lowers the number of layers developed in the liquid, making heat transfer easier.

4.4 Heat Transfer with a magnetic field

The magnetic influence on heat transmission will be discussed in the next part by utilizing the Nusselt number for the four scenarios compared above.

The case when all walls are electrically insulating (walls- EI) is shown in Fig. 6(a), which clarified the evolution of the average Nusselt number as Ha increases for various Ri

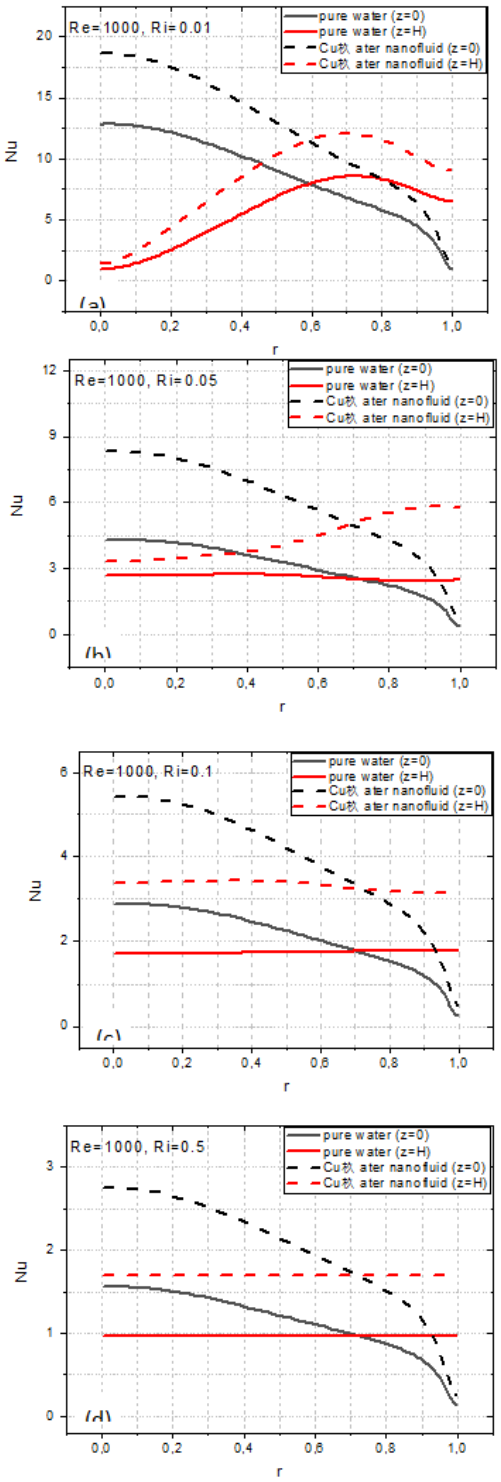

Fig. 4. Comparison of Local Nusselt number between pure Water and nanofluid for different Ri.

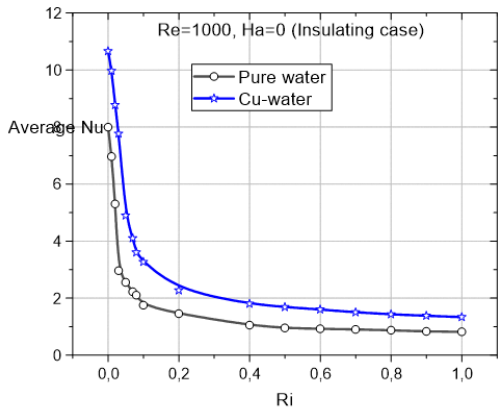

Fig.5. Effect of the Richardson number on the average Nusselt number;

When Ri=0, the maximum value of Nu for Ha=0 is obtained, indicating the supremacy of forced convection. The meridian flow has a single big cell in this scenario. The magnetic field effect in this scenario is unsatisfactory since it reduces the Nusselt number. The laminated layers that insulate the heated lid reduce heat transmission even in the presence of a strong magnetic field. When the conduction mode dominates heat transmission, the average Nusselt number drops as *Ri* rises [47-49].

When the enclosure walls are completely electrically conducting, the Hartmann layer is suppressed under boundary circumstances (walls -EC). As a result, this process serves to remove more layers of fluid, increasing heat transmission. The latter is represented by the average Nusselt number, which changes as Ha grows. In (Fig.6b), the average Nusselt number is displayed as a function of Ha for various Ri. Nusselt number Nu rises and reaches a maximum of 17.1 for Ha18 and Ri= 0. When the Ha is increased further, the Nusselt curve is flipped, and it gradually lowers until it finds equilibrium between the electromagnetic and viscous forces.

Fig. 6c depicts the fluctuation of the average Nusselt number with increasing Ha and for varying Ri in the (bottom -EC) example (c). The minimal heat transfer for the lower Ha is determined in this figure. Average Nusselt is a rising function of Ha ≤25 and a decreasing function of Ha when 30≤Ha<60, however, it decreases with increasing Ri.

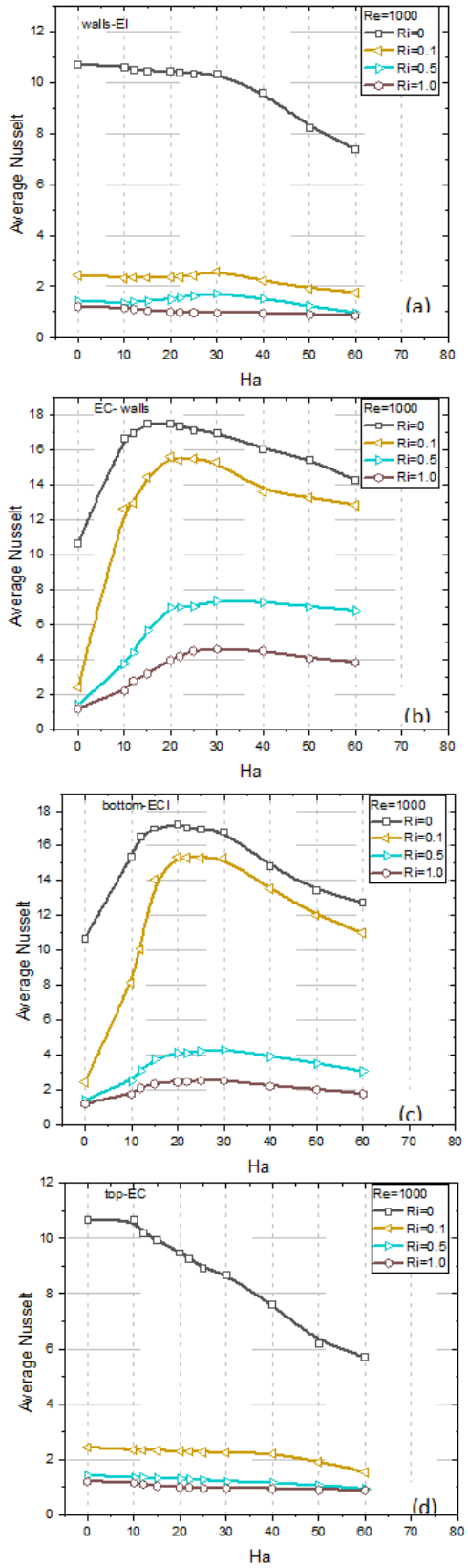

Fig .6. Effect of Hartmann number on the local Nusselt number for the case of Ri=0.04

When Ha rises, the average Nu rises as well, peaking at Ha≈22 for $0 \leq Ri \leq 0.1$ and Ha=30 for Ri=1. Increases in Ha have the reverse impact on heat transmission since the mean Nusselt drops from Ha 30 to Ha = 60.

The introduction of a magnetic field while the top disk is electric conducting (Top-EC) results in no improvement in heat transmission, as demonstrated by the average Nusselt number in Fig. 6(d).

5. Conclusions

The influence of electrical conductivity walls on heat transfer of nanofluid swirling flow through cylindrical containers under an axial magnetic field was investigated. The four scenarios examined in this study are as follows: (EI-walls), (Walls-EC), (Bottom-EC), and (Top-EC).The main conclusions are:

- The stratified layers increase with increasing buoyancy force, which forms an insulating layer between the hot zone and the cold zone which will reduce the heat transfer.
- The reduction in the number of nanofluid layers is related to the increase in Nusselt number values.
- The best heat transfer is obtained when the walls are all electrically conductive, in which case a 100% improvement is observed at low Richardson numbers.
- The average Nusselt number increases when reaching equilibrium between the electromagnetic force and the viscous force.
- The electrical conductivity of the walls of the enclosure which contains the nanofluid is necessary to maintain a high heat transfer in the swirling flows.

Acknowledgment

The authors gratefully acknowledge the support of the General Directorate of Scientific Research and Technological Development (DGRSDT - Algeria).

References

[1] B. Mahfoud, Effect of Wall Electrical Conductivity on Heat Transfer Enhancement of Swirling Nanofluid Flow, Journal of Nanofluids 12(2) (2023) 418-428.

[2] S.M. Aminossadati, B. Ghasemi, Natural convection cooling of a localised heat source at the bottom of a nanofluid-filled enclosure, European Journal of Mechanics B/Fluids (28) (2009) 630–640.

[3] M. Sheikholeslami, M. Hatami, D.D. Ganji, Nanofluid flow and heat transfer in a rotating system in the presence of a magnetic field, Journal of Molecular Liquids (2014) (190) 112–120.

[4] H. Shafiee, E. NikzadehAbbasi, M. Soltani, Numerical Study of the Effect of Magnetic Field on Nanofluid Heat Transfer in Metal Foam Environment, HindawiGeofluids 3209855 (2021) 14 pages.

[5] M. Sheikholeslami, M. Jafaryar, Thermal assessment of solar concentrated system with utilizing CNT nanoparticles and complicated helical turbulator, International Journal of Thermal Sciences 184 (2023) 108015.

[6] M. Sheikholeslami, Numerical investigation of solar system equipped with innovative turbulator and hybrid nanofluid, Solar Energy Materials and Solar Cells (243) (2022) 111786.

[7] M. Sheikholeslami, Analyzing melting process of paraffin through the heat storage with honeycomb configuration utilizing nanoparticles, Journal of Energy Storage 52 (Part B) (2022) 104954.

[8] M. Sheikholeslami, Numerical analysis of solar energy storage within a double pipe utilizing nanoparticles for expedition of melting, Solar Energy Materials and Solar Cells (245) (2022) 111856.

[9] M. Sheikholeslami, Modeling investigation for energy storage system including mixture of paraffin and ZnOnano-powders considering porous media, Journal of Petroleum Science and Engineering (219) (2022) 111066.

[10] M. Sheikholeslami, Z. Ebrahimpour, Thermal improvement of linear Fresnel solar system utilizing Al2O3-water nanofluid and multi-way twisted tape, International Journal of Thermal Sciences, (176) (2022) 107505.

[11] M. Sheikholeslami, M. Jafaryar, Performance of energy storage unit equipped with vase-shaped fins including nanoparticle enhanced paraffin, Journal of Energy Storage (58) (2023) 106416.

[12] B. Mahfoud, A. Bendjaghlouli, Natural convection of a nanofluid in a conical container, Journal of Thermal Engineering 4(1) (2018) 1713–1723.

[13] B. Mahfoud., H. Benhacine, A. Laouari, A. Bendjaghlouli, Magnetohydrodynamic Effect on Flow Structures Between Coaxial

Cylinders Heated from Below, Journal of Thermophysics and Heat Transfer 34(2) (2019) 1-10.

[14] B. Mahfoud, A. Laouari, A. Hadjadj, H. Benhacine, Counter-rotating flow in coaxial cylinders under an axial magnetic field, European Journal of Mechanics-B/Fluids (78) (2019) 139-146.

[15] A. Bendjaghlouli ,B. Mahfoud, D.E. Ameziani , Magnetohydrodynamic flow in a truncated conical enclosure, Journal of Thermal Engineering(5) (2019) 77-83.

[16] A. Bendjaghlouli, D.E. Ameziani, B. Mahfoud, L. Bouragbi, Magnetohydrodynamic Counter Rotating Flow and Heat Transfer in a Truncated Conical Container, Journal of Thermophysics and Heat Transfer 33(3) (2019) 365-374.

[17] A. Laouari, B. Mahfoud, R. Bessaïh, A. Hadjadj, Hydrodynamic instabilities in swirling flow under axial magnetic field, European Journal of Mechanics-B/Fluids (85) (2021) 245–260.

[18] H.F. Öztop, H. Coşanay, F. Selimefendigil, N. Abu-Hamdeh, Analysis of melting of phase change material block inserted to an open cavity, International Communications in Heat and Mass Transfer (137) (2022) 106240.

[19] N. Ugurlubilek, Z. Sert, F. Selimefendigil, H. F. Öztop, 3D laminar natural convection in a cubical enclosure with gradually changing partitions, International Communications in Heat and Mass Transfer (133) (2022) 105932.

[20] F. Selimefendigil, H.F. Öztop, Thermal management and performance improvement by using coupled effects of magnetic field and phase change material for hybrid nanoliquid convection through a 3D vented cylindrical cavity, International Journal of Heat and Mass Transfer 183(Part C) (2022) 122233.

[21] H. Berrehal, S. Dinarvand, I. Khan, Mass-based hybrid nanofluid model for entropy generation analysis of flow upon a convectively-warmed moving wedge, Chinese Journal of Physics (77) (2022) 2603-2616.

[22] S. Dinarvand, H. Berrehal, I. Pop, A.J. Chamkha, Blood-based hybrid nanofluid flow through converging/diverging channel with multiple slips effect: a development of Jeffery-Hamel problem, International Journal of Numerical Methods for Heat & Fluid Flow 33(3) (2023) 1144-1160.

[23] S. Dinarvand, S.M. Mousavi, M.Yousefi, M. Nademi Rostami, MHD flow of MgO-Ag/water hybrid nanofluid past a moving slim needle considering dual solutions: an applicable model for hot-wire anemometer analysis, International Journal of Numerical Methods for Heat & Fluid Flow 32 (2) 488-510.

[24] S. Dinarvand, M. Yousefi, A.J. Chamkha, Numerical Simulation of Unsteady Flow toward a Stretching/Shrinking Sheet in Porous Medium Filled with a Hybrid Nanofluid, Journal of Applied and Computational Mechanics8(1) *(*2022) 11-20.

[25] S. Dinarvand, A.M. Nejad, Off-centered stagnation point flow of an experimental-based hybrid nanofluid impinging to a spinning disk with low to high non-alignments, International Journal of Numerical Methods for Heat & Fluid Flow, 32(8) (2022) 2799-2818.

[26] M. Mansourian ,S. Dinarvand, I. Pop ,Aqua Cobalt Ferrite/Mn–Zn Ferrite Hybrid Nanofluid Flow Over a Nonlinearly Stretching Permeable Sheet in a Porous Medium , Journal of Nanofluids 11(3) (2022) 383-391.

[27] M. Izady, S. Dinarvand, I. Pop, A.J. Chamkha, Flow of aqueous Fe2O3–CuO hybrid nanofluid over a permeable stretching/shrinking wedge: A development on Falkner–Skan problem, Chinese Journal of Physics, (74) (2021) 406-420.

[28] G. Amirhossein, S. Dinarvand, A. Adamian, M.A , Sheremet, Unsteady General Three-Dimensional Stagnation Point Flow of a Maxwell/Buongiorno Non-Newtonian Nanofluid, Journal of Nanofluids, (8) (2019) 1544-1559.

[29] B. Jabbaripour, M. N. Rostami, S. Dinarvand, I. Pop, Aqueous aluminium–copper hybrid nanofluid flow past a sinusoidal cylinder considering three-dimensional magnetic field and slip boundary condition, Proceedings of the Institution of Mechanical Engineers, Part E: Journal of Process Mechanical Engineering,October 12 (2021).

[30] B. Mahfoud, Simulation of Magnetic Field Effect on Heat Transfer Enhancement of Swirling Nanofluid, International Journal of Computational Materials Science and Engineering 11(4) (2022) 2250007.

[31] B. Mahfoud, Enhancement Heat Transfer of Swirling Nanofluid Using an Electrical Conducting Lid**,** Journal of Thermophysics and Heat Transfer (37) (2023) 263-271

[32] L. Bouragbi, A. Salaheddine, B. Mahfoud, Analyses of entropy generation for a solar

minichannel flat plate collector system using different types of nanofluids, Journal of Computational Applied Mechanics 52(4) (2021) 664-681.

[33] B. Mahfoud, Magnetohydrodynamic effect on vortex breakdown zones in coaxial cylinders, European Journal of Mechanics-B/Fluids (89) (2021) 445–457.

[34] Y. Slatni, T. Messai, B. Mahfoud, Numerical simulation of thermal behavior in a naturally ventilated greenhouse, International Journal of Computational Materials Science and Engineering 11 (2022) 2150034 .

[35] B. Mahfoud, Effects of an Axial Magnetic Field on Vortex Breakdown and Fluid Layer, Journal of Applied Fluid Mechanics 14(6) (2021) 1741–1753.

[36] H. Benhacine, B. Mahfoud, M. Salmi ,Stability effect of an axial magnetic field on fluid flow bifurcation between coaxial cylinders, International Journal of Computational Materials Science and Engineering 10(4) (2021) 2150023.

[37] H. Benhacine, B, Mahfoud, M. Salmi, Stability of conducting fluid flow between coaxial cylinders under thermal gradient and axial magnetic Field, International Journal of Thermofluid Science and Technology 9(2) (2022) 090202.

[38] B. Mahfoud, A. Bendjaghlouli, R. Bessaïh, Magneto-hydrodynamic co-rotating flow in a vertical cylindrical container, Numer. Heat Transfer 69(12) (2016) 1051-1063.

[39] B. Mahfoud, R. Bessaïh, Magnetohydrodynamic counter-rotating flow in a cylindrical cavity, International Journal of Heat and Mass Transfer (93) (2016) 175–185.

[40] S.P.A. Devi, S.S.U. Devi, Numerical Investigation of Hydromagnetic Hybrid Cu – Al2O3/Water Nanofluid Flow over a Permeable Stretching Sheet with Suction, International Journal of Nonlinear Sciences and Numerical Simulation 17(5) (2016) 249-257.

[41] A.J. Chamkha, I. V. Miroshnichenko, M. A. Sheremet, Numerical analysis of unsteady conjugate natural convection of hybrid water-based nanofluid in a semicircular cavity, Journal of Thermal Science and Engineering Applications (9) (2017) 041004.

[42] M. Mollamahdi, M. Abbaszadeh, G. A. Sheikhzadeh, Flow field and heat transfer in a channel with a permeable wall filled with Al2O3-Cu/water micropolar hybrid nanofluid, effects of chemical reaction and magnetic field, Journal of Heat and Mass Transfer Research (JHMTR) (3) (2016) 101 114.

[43] M.A. Mansour, S. Sadia, R. Gorla , A.M. Rashad, Effects of heat source and sink on entropy generation and MHD natural convection of Al2O3-Cu/water hybrid nanofluid filled with square porous cavity, Thermal Science and Engineering Progress (6) (2017) 57-71.

[44] M. Aghamajidia, M.E. Yazdi, S. Dinarvand, I. Pop, Tiwari-Das nanofluid model for magnetohydrodynamics (MHD) natural-convective flow of a nanofluid adjacent to a spinning down-pointing vertical cone, Propulsion and Power Research (7) (2018) 78-90.

[45] S. Boulkroune, O. Kholai, B. Mahfoud, Effects of Important Parameters on the transition from forced to mixed convection flow in a square cavite, Defect and Diffusion Forum 406 (2021) 36-52.

[46] S. Patankar, Numerical Heat Transfer and Fluid Flow, McGraw-Hill, 2018. (New-York)

[47] B. Mahfoud, R. Bessaïh, Stability of swirling flows with heat transfer in a cylindrical enclosure with co/counter-rotating end disks under an axial magnetic field. Numerical Heat Transfer, Part A,61(6) (2012). 463-482 .

[48] B. Mahfoud, R. Bessaïh, Oscillatory swirling flows in a cylindrical enclosure with co-/counter-rotating end disks submitted to a vertical temperature gradient, Fluid Dynamics &MaterialsProcessing *8*(1), (2012), 1-26.

[49] B. Mahfoud, Hibet.E. Mahfoud, Behaviors of Vortex Breakdown in Steady-State and Oscillatory Flow under an Axial Magnetic, *Researchgate.net/publication (*2023).